SCIENTIFIC REPORTS

OPEN

Reliable charge assessment on encapsulated fragment for endohedral systems

Received: 27 October 2017
Accepted: 1 February 2018
Published online: 13 February 2018

A. J. Stasyuk[1], M. Solà[1] & A. A. Voityuk[1,2]

A simple scheme to determine charge distribution in endohedral complexes is suggested. It is based on comparison of inner-shell atomic orbital energies of the encapsulated species to the corresponding energies in reference systems with unambiguously defined charges on X. This robust approach is applied to endohedral borospherenes X@B_{39}, for which the conventional schemes provide in some cases quite different results. Efficiency of proposed scheme also has been proven for typical fullerene based Sc_3N@C_{80} endohedral complex.

Atomic charge is one of the most widely used concepts in chemistry. But, it can unambiguously be defined only in some trivial cases. For instance, in homogeneous diatomic molecules with the total charge Q, the charge on each atom is equal to Q/2. In general, however, some assumptions should be made in order to quantify the charge distribution in a molecular system. Many different schemes to define atomic charges have been developed. Most popular of them are schemes based on the distribution of the electron density obtained from quantum-mechanical calculation and its subsequent transformation into atomic charges –Mulliken[1], Lowdin[2], Hirshfeld[3], CM5[4], Weinhold[5,6] (natural population analysis, NPA), and Bader[7,8] (quantum theory of atoms in molecules, QTAIM) population analysis.

Discovery of buckminsterfullerene C_{60}[9], and its La encapsulated derivative[10–12] made a new milestone in chemistry. Fullerenes containing confined atoms or small molecules are called endohedral fullerenes (EFs). Most often the incarcerated species is a metal atom or metallic cluster, and such systems are called endohedral metallofullerenes (EMFs)[13–22]. Charge transfer between the encapsulated species and the cage in EMFs is important because it determines the most suitable cage among the many possible isomers. For instance, in Sc_2C_2@C_{68} with a formal charge transfer of 4 electrons, the cage corresponds to the 6073 isomer[23], whereas the cage that encapsulates Sc_3N@C_{68} with a formal charge of 6 electrons is the 6140[24]. Although many EMFs have been intensively studied they continue to attract much attention of researchers from various fields of natural sciences. Recent discovery by Zhai *et al.* of all-boron fullerenes B_{40}^- and B_{40}^0 (referred in literature as borospherenes)[25] has given a new impetus to the chemistry of endohedral compounds and stimulated a large number of experimental and theoretical studies. A few months later Bai *et al.* studied computationally the viability of endohedral metalloborospherenes M@B_{40} (M = Ca, Sr). DFT calculations revealed great stability due to the almost perfect match in size of encapsulated fragment and cage. It was found that all these metalloborospherenes are formally charge-transfer $M^{2+}B_{40}^{2-}$ complexes[26]. Other endohedral complexes of borospherenes based on B_{36}^-[27], B_{38}^{2-}[28], and B_{39}^-[29], cages demonstrate similar behaviour. A number of works predicting the existence of endohedral borospherenes have been published very recently[30–34]. Making an analogy with carbon fullerenes we can expect that endohedral borospherenes will be synthetized at an early date.

Results and Discussions

Focusing our attention on endohedral Cl@B_{39} borospherene complex based on B_{39} cage subunit, we have encountered the problem of the reliability of charge determination on central fragment. The population analysis carried out within various schemes demonstrates significantly different distribution of charges. However, a reliable definition of the charge localized on the encapsulated fragment as well as its changes is important for the understanding of chemical reactivity, and, in particular, for photo-induced charge transfer (CT) process in endohedral compounds[35–38].

[1]Institut de Química Computacional and Departament de Química, Universitat de Girona, C/ Maria Aurèlia Capmany 69, 17003, Girona, Catalonia, Spain. [2]Institució Catalana de Recerca i Estudis Avancats, 08010, Barcelona, Spain. Correspondence and requests for materials should be addressed to A.J.S. (email: antony.stasuk@gmail.com) or M.S. (email: miquel.sola@udg.edu) or A.A.V. (email: alexander.voityuk@gmail.com)

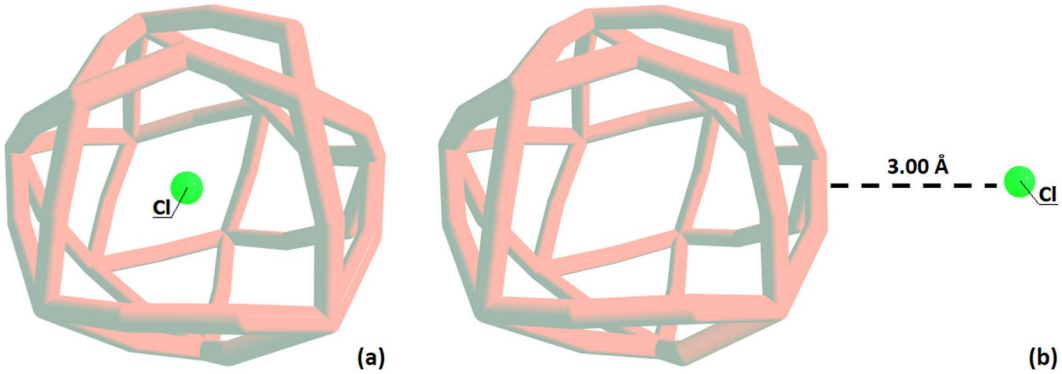

Figure 1. Graphical representation of endohedral boroshperene complex Cl@B_{39} (**a**) and (B_{39} + Cl) vdW complex (**b**).

	Mulliken	Löwdin	Hirshfeld	CM5	QTAIM	NPA
	Cl@B_{39}					
B_{39}	0.111	−0.758	−0.002	−0.114	0.658	0.560
Cl	−0.111	0.758	0.002	0.114	−0.618	−0.560
	(B_{39} + Cl) vdW					
B_{39}	0.410	0.239	0.393	0.385	0.580	0.480
Cl	−0.410	−0.239	−0.393	−0.385	−0.547	−0.480

Table 1. Charge density analysis (in electrons) performed with Mulliken, Löwdin, Hirshfeld, CM5, QTAIM, and Natural Population Analysis (NPA) schemes for endohedral Cl@B_{39} and (B_{39} + Cl) van der Waals (vdW) complex obtained at PBE0/Def2-TZVP level of theory. Total charge is in all cases zero.

In this work, we present a new scheme for assessment of charge distribution on endohedral complexes. Proposed method is based on straightforward physical model and could be used as a convenient tool for the culling of inadequate charge schemes. All calculations were performed with the PBE0/Def2-TZVP (with ECP-28 and ECP-60 for Ag and Au atoms[39] correspondently) method[40–42] using Gaussian 09 program[43].

Numerous proofs that metal-encapsulating borospherenes could demonstrate remarkable charge transfer properties have been recently reported. Among them, the work published by Chen *et al.*[29] demonstrates at first-principles level the viability of the axially chiral metalloborospherenes Ca@B_{39}^{+}. At the same time there are no examples of halogen encapsulated borospherenes, despite the fact that such complex is a unique system of halogen encapsulate into superhalogen unit. The uniqueness of the Cl@B_{39} complex is that both fragments exhibit high electron affinity (Cl – 3.612 eV[44], B_{39} – 3.845 eV[45]). Thus it seems extremely difficult to predict charge distribution in such system. With a certain degree of confidence it can be assumed that charge separation should be observed, however it is completely unclear which of the fragments will be negatively charged and which positively.

Charge distribution analysis for B_{39} boroshperene complexes. We focused our attention on complexes such as Cl@B_{39} (Fig. 1a), in particular on the description of charge states in such systems using various approaches. We found that charges on internal fragment, as well as on the cage, depend dramatically on the population scheme used.

In contrast, for van der Waals complex (Fig. 1b) composed of B_{39} and Cl separated by 3 Å, (B_{39} + Cl) vdW, the predicted charges demonstrate a significant similarity (Table 1).

As can be seen from Table 1, for Cl@B_{39} complex, charge on the Cl fragment can vary from −0.62 e (QTAIM) to 0.76 e (Löwdin) depending on the used scheme. At the same time, charge on the cage ranges from −0.76 e (Löwdin) to 0.66 e (QTAIM). Presuming that behaviour of these fragments in endohedral complex does not change significantly, the reliability of the charges obtained based on Löwdin population analysis ($Q_{Cl} = 0.76$), as well as on Hirshfeld ($Q_{Cl} = 0.00$) and CM5 ($Q_{Cl} = 0.14$) schemes should be called into question. For the van de Waals complex, the obtained charge values on the Cl atom are much closer to each other and vary from −0.24 e (Löwdin) to −0.58 e (QTAIM).

The main problem in this case is the selection of the most reliable method/scheme of charge assessment, which is almost impossible without resorting to chemical intuition.

Model description. It is well known that the ionization potential (binding energy) of the inner-shell electrons of an atom in a molecular system depends on the charge state and chemical surroundings of the atom[46]. A linear relationship of the binding energy (E_b) measured by X-ray photoelectron spectroscopy (XPS) and an atomic charge q computed with quantum mechanical methods (Eq. (1)) was established for different classes of chemical compounds

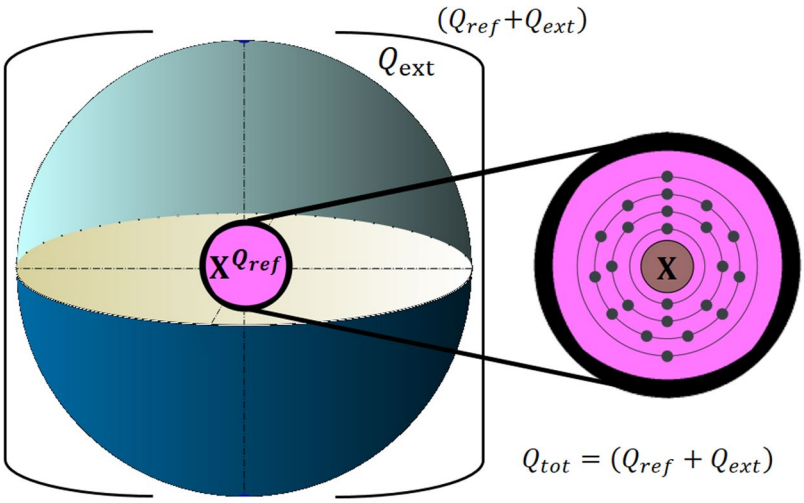

Figure 2. Physical model used in this work.

$$\Delta E_b = E_b - E_{b0} \approx Aq \tag{1}$$

The XPS shift ΔE_b is determined with respect to the binding energy E_{b0} found for a reference. Further studies showed, however, that the electrostatic potential φ created by chemical surroundings has to be accounted for[47]

$$\Delta E_b = Aq + \varphi \tag{2}$$

There are inherent physical limitations that prevent accurate determination of the atomic charges. In particular, the parameters q and φ in Eq. (2) refer to the ground electronic state of the system, while the measured XPS shift, ΔE_b, reflects both the ground and the final excited state (with a hole in the inner shell). To separate the contributions Aq and φ, some additional assumptions should be used. In spite of these and some other restrictions, XPS has been widely employed for chemical analysis[48].

Let's consider a model system consisting of a multi-electron fragment X with partial charge Q_{ref} incorporated into a cage constructed of N atoms with partial charge Q_{ext} (Fig. 2).

Similar to Eq. (2) we assume that the orbital energy of core electrons of an atom of fragment X (X consists of either a single atom or several atoms) can be approximately presented as a simple function of the charge Q_X *on fragment* X, corrected by the external electrostatic potential φ_{ex} on atom due to the cage

$$\varepsilon_k^{corr}(Q_x, \varphi_{ext}) = \varepsilon_k(Q_x) + \varphi_{ext} \tag{3}$$

The non-trivial point here is how to calibrate $\varepsilon_k^{corr}(Q_x, \varphi_{ex})$ so that the charge Q_X in the reference systems is uniquely defined.

We propose the following step-by-step scheme to derive the charge on X in X@Cage species:

1. One constructs reference systems where charge on X is unambiguously defined. The reference systems for such a situation include the fragment X carrying the total charge Q_{ref} (e.g. $Q_{ref} = -1, 0, +1$ *etc*) embedded into a sphere having the charge Q_{ext}. The total charge Q_{tot} of the reference system, $Q_{tot} = Q_{ref} + Q_{ext}$, is equal to the charge of X@Cage. In most cases X@Cage is neutral ($Q_{tot} = 0$) and thus for any reference system $Q_{ext} = -Q_{ref}$. If X@Cage is charged, $Q_{ext} = Q_{tot} - Q_X$. The radius of the sphere R is determined by the cage geometry. For a cage comprising N atoms, R can be defined as

$$\frac{1}{R} = \frac{1}{N}\sum_{i=1}^{N}\frac{1}{r_i} \tag{4}$$

where r_i is the distance from atom i in the cage to the center of the cage determined by the non-*weighted* mean of the coordinates of the atoms in the cage. In this approach:

$$\varphi_{ext} = \frac{Q_{ext}}{R} \tag{5}$$

2. Quantum mechanical calculation with molecular charge Q_{ref} (e.g. $Q_{ref} = -1, 0, +1$, *etc.*) are carried out. The computed orbital energy of inner shell K, $\varepsilon_K(Q_{ref})$, together with the electrostatic potential created by the sphere provides $\varepsilon_K^{corr}(Q_{ref})$:

$$\varepsilon_K^{corr}(Q_{ref}) = \varepsilon_K(Q_{ref}) + \frac{Q_{ext}}{R} \tag{6}$$

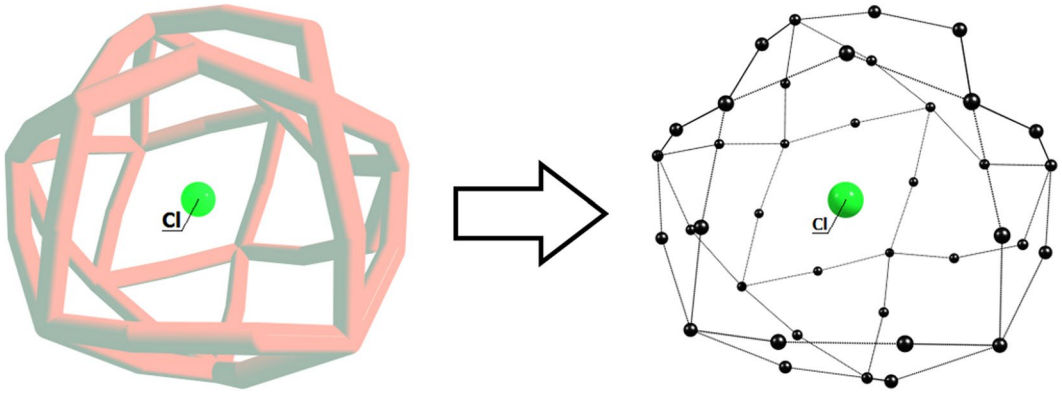

Figure 3. Transformation of $Cl@B_{39}$ complex within the point charge model framework necessary for calibration curve construction. Left part of figure corresponds to $Cl@B_{39}$ complex, right part represents central fragment (Cl) surrounded by compensation charges (black spheres) allocated at former boron nuclei places.

The found values ε_K^{corr} are used to obtain a quadratic interpolation of the $\varepsilon_K^{corr}(Q_{ref})$ dependence. Note that the encapsulated species X comprise usually only several atoms and its calculation is very fast.

3. Quantum mechanical calculations of X@Cage provide the ε_K value in the "real" system. Using the interpolated function $\varepsilon_K^{corr}(Q_{ref})$ derived in the previous step we could directly obtain the charge Q_X on the encapsulated fragment.

These three steps represent the simplest scheme to estimate charge separation between encapsulated species X and the cage in endohedral fullerenes and in similar structures. As shown below, a more elaborated treatment of the electrostatic embedding in the reference systems does not provide significantly different results. Also, as we will see, the proposed scheme is quite robust to choosing the inner shell *K* in X when constructing the interpolated function $\varepsilon_k^{corr}(Q_{ref})$.

The classical point charge model was used to evaluate the electrostatic correction. This model implies the replacement of cage atoms by array of point charges placed at the nuclei of the constituted atoms. This approach has proven itself well in various fields of chemical science and computational biology[49,50].

To verify the applicability of the proposed model to the charge assessment of the central fragment in endohedral complexes, the borospherene species $Cl@B_{39}$ was considered in detail (Fig. 3).

Primary, it is necessary to perform a series of calculations for Cl fragment in various charge states. For this we have selected 5 states – Cl^{2-}, Cl^{1-}, Cl^{0}, Cl^{1+}, and Cl^{2+} in their ground states. Despite the fact that Cl^{2+} as well as other halogen cations goes beyond conventional chemical principles and its existence is apparently impossible under ordinary conditions, we will take it into account as a model point to have a wider range of calibration. Including a large set of charge states into calibration makes a proposed scheme more robust and universal due to the fact that even in difficult cases a result can be found within the interpolation grid. Of course, in case of Cl fragment, data about its possible charge states is well known, but in case of more sophisticated encapsulated unit a necessary information can simply not be available. Moreover, it was found that inclusion of 1s orbital energy of Cl^{2+} unit does not lead to physically meaningless result, therefore we recommend to use greater number of charge states for constructing a calibration curve.

To take into account correction to electrostatic potential, boron atoms forming cage have to be replaced with point charges (Fig. 3) in such way that total compensation charge has to be equal to the charge on Cl fragment in current charge state. For example, for Cl^{1+} cation compensation charge have to be equal to -1, while for Cl^{1-} fragment the compensation charge have to be equal to $+1$. It seems obvious that there are more than one way of the compensation charge distribution over cage nodes when the neutrality condition is satisfied.

To investigate the effect of compensation charge distribution on 1s orbital energy we performed calculations for 4 different models (Table S1, ESI). To construct first of them, even charge distribution over the cage were used, while for Cl^0 charge state no compensation point charges have been applied (CCS1, Table S1). In next three schemes, the charges on cage were generated randomly to compensate the charge -1 and then be linearly scaled to the charge state -2. In the case of Cl^{1+} and Cl^{2+}, compensation charges on the cage were obtained from previously generated only with opposite sign (CCS2, CCS3, and CCS4 in Table S1). Last scheme is characterized by random generation of charges on all cage nodes for each state of Cl fragment. Only equality of the charge on Cl fragment and sum of compensation charges was monitored (CCS5, Table S1). Calibration curves and equations of approximate functions are shown in Fig. S1. Detailed analysis of given charge distribution schemes revealed that electrostatic correction for 1 s orbital energy value depends only very weakly on particular compensation charge scheme. For the studied charge distributions, the range of the correction values is about one order of magnitude less than the correction values themselves (Table S2). At the same time, central fragment charges predicted on the basis of the mentioned charge compensation schemes are in the range from -0.44 e to -0.51 e. Thus, taking into account small differences in charge prediction caused by particular charge compensation method, we will use the even charge distribution as a compensation method.

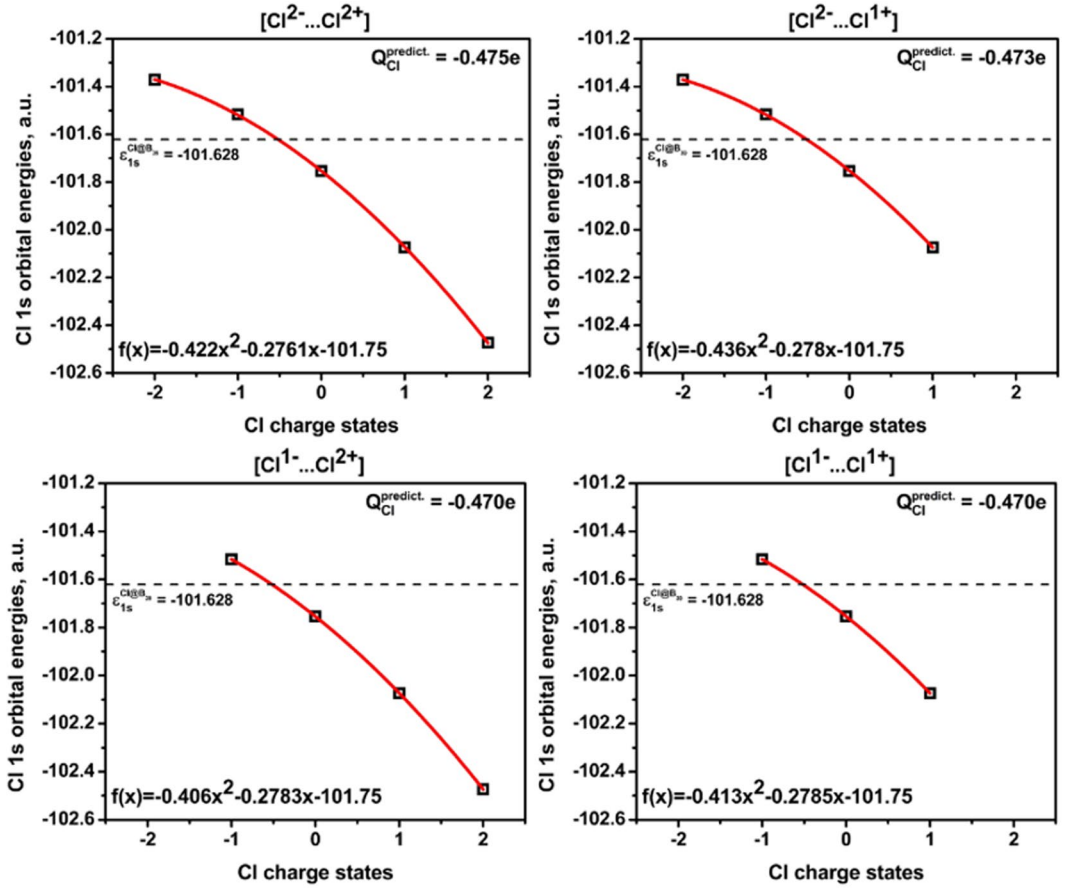

Figure 4. Calibration curves constructed using various number of reference points (top left – $[Cl^{2-}…Cl^{2+}]$ – 5 points, top right – $[Cl^{2-}…Cl^{1+}]$ – 4 points, bottom left – $[Cl^{1-}…Cl^{2+}]$ – 4 points and bottom right – $[Cl^{1-}…Cl^{1+}]$ – 3 points) for charge prediction on central Cl fragment in $Cl@B_{39}$ complex (Cl 1s orbital energy in complex of interest = −101.628 a.u.).

At the next stage of our work, we studied the effect of the charge states taken into consideration on the predicted charge values of the $Cl@B_{39}$ complex. It was found that the charge predicted within the proposed method depends weakly on charge states of Cl fragments that were taken into account in calibration. Four different calibration curves were built using various Cl charge states – 1st: $[Cl^{2-}…Cl^{2+}]$ with 5 reference points (Q_{Cl} = −0.475), 2nd: $[Cl^{2-}…Cl^{1+}]$ with 4 points (Q_{Cl} = −0.473), 3rd: $[Cl^{1-}…Cl^{2+}]$ with 4 points (Q_{Cl} = −0.470), and 4th: $[Cl^{1-}…Cl^{1+}]$ with 3 points (Q_{Cl} = −0.470) (Fig. 4).

As can be seen in Fig. 4, minor differences (of less than 0.01 e) in the predicted charge on the Cl fragment obtained from different calibration curves are found. This error is one order of magnitude smaller than the error caused by the use of different charge compensation schemes.

Thus, we can conclude that for studied $Cl@B_{39}$ complex proposed method has shown its best side. However, we were wondering if proposed method can equally work well with other K-type orbitals. To check this, $Cu@B_{39}$ complex has been considered. Cu atom has 3 inner s-orbitals. Calibrations curves construct for 1s, 2s, and 3s orbitals based on five Cu charge states $[Cu^{2-}…Cu^{2+}]$ reference points predict charge on central fragment 0.416 e, 0.391 e, and 0.398 e correspondently (Fig. S2, ESI). Thus, one can assume that any inner orbital, as far as it not involved in any orbital interaction with the cage orbitals, could be used for construction of the calibration. The latest suggests that the proposed scheme can be extended to "heavy" elements, for which pseudopotentials are used.

Model verification. Finally, to verify the proposed approach several systems with general formula $X@B_{39}$, where X represents halogens (F, Cl, Br), small radicals (NO, CN, FO, CF) or metals of 1B group of periodic chart (Cu, Ag, Au) were investigated (Fig. S3). The summary results are presented in Table 2.

As can be seen from Table 2, the proposed charge assessment approach provides the physically adequate results in all studied cases. For each cases, Mulliken and Löwdin charge assessment schemes provide the worst performance with correlations with the Q_X predicted charges of $R^2 = 0.388$ for Mulliken and $R^2 = 0.172$ for Löwdin, respectively. Moreover, sometimes they provide physically meaningless results, such as in case of $Au@B_{39}$ (Mulliken) or $Cl@B_{39}$, $Br@B_{39}$, $FO@B_{39}$ and $CN@B_{39}$ (Löwdin) complexes. Hirshfeld charges are quite well correlated with the predicted charges ($R^2 = 0.909$) but the charges are noticeably underestimated. CM5 method yields comparable to Hirshfeld correlation with the predicted results with $R^2 = 0.896$. Equally to Hirshfeld scheme, significant charge underestimation for CM5 is observed. In some cases Hirshfeld and CM5 schemes does not

X	Mulliken	Löwdin	Hirshfeld	CM5	NPA	AIM	Q_X predict.[a]
F	−0.603	−0.300	−0.334	−0.305	−0.842	−0.822	−0.585 (1s F)
Cl	−0.111	0.758	0.002	0.114	−0.560	−0.618	−0.475 (1s Cl)
Br	−0.326	1.142	0.209	0.417	−0.258	−0.357	−0.251 (1s Br)
NO	0.444	0.842	0.458	0.473	0.127	0.030	0.212 (1s O) 0.253 (1s N)
CN	−0.793	0.162	−0.177	−0.117	−1.070	−0.899	−0.763 (1s N) −0.841 (1s C)
FO	−0.267	0.297	0.027	0.085	−0.532	−0.619	−0.252 (1s F) −0.356 (1s O)
CF	0.014	0.865	0.472	0.582	0.001	0.086	0.176 (1s F) 0.257 (1s C)
Cu	0.187	0.306	0.487	0.825	0.754	0.719	0.416 (1s Cu) 0.391 (2s Cu) 0.398 (3s Cu)
Ag	0.142	0.620	0.506	0.984	0.738	0.586	0.443 (4s Ag)
Au	−0.589	0.705	0.560	0.972	0.799	0.417	0.441 (5s Au)

Table 2. Charge density analysis performed with Mulliken, Löwdin, Hirshfeld, CM5, QTAIM, and NPA schemes for endohedral X@B_{39} complex and the predicted charge of X (Q_x predicted)[a] obtained within the method proposed in this work. Units are electrons. [a]Information in brackets refer to the atoms and orbitals used for calibration.

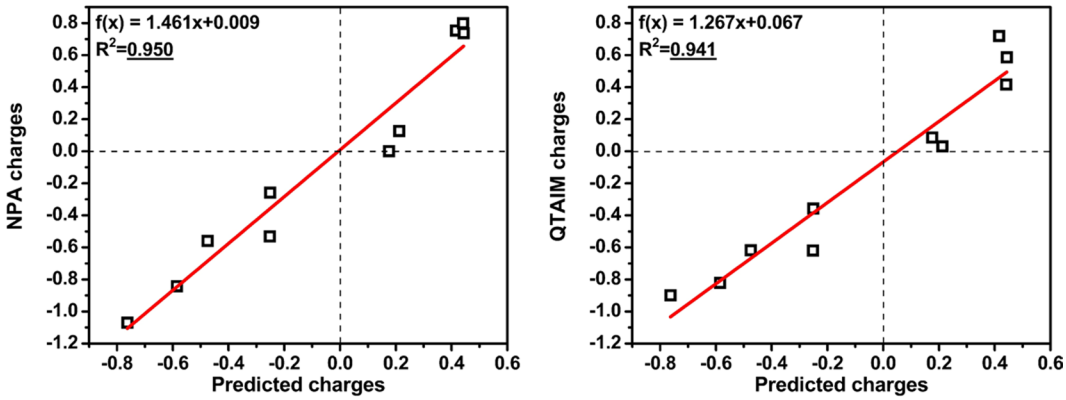

Figure 5. Correlations of the NPA and QTAIM charges with the results obtained by the proposed method. Units are electrons.

reproduce the sign of charge on the central fragment (Fig. S4, Table S3, ESI). Finally, the best correlations between calculated and predicted charges were found for NPA and QTAIM schemes (Fig. 5).

Thus, we can conclude that the predicted charge assessment method provide results comparable with well-known methods and can be used as a fast and convenient selection tool that avoids assignment of unphysical charges to encapsulated species.

To demonstrate that the proposed method can be applied not only to boron cages but also to a wide range of endohedral compounds, one of the most studied (both synthetically[51–53] and theoretically[54,55]) $Sc_3N@I_h$-C_{80} cluster has been investigated. Detailed charge distribution analysis within Mulliken, Löwdin, Hirshfeld, CM5, QTAIM, and NPA schemes has been performed. For $Sc_3N@I_h$-C_{80} complex, calculated charge values on the Sc_3N fragment vary from −0.090 e obtained with Mulliken scheme to 0.851 e and 0.969 e for Löwdin and Hirshfeld ones, correspondently. CM5 scheme provides 2.062 e, while NPA and Bader analysis result in 3.426 e and 3.772 e (for more details see ESI). Scheme proposed in current paper predicts the charge on central fragment of 1.502 e based on 1s N orbitals calibration. Thus, with this latter example we show that encapsulated fragment charge estimation scheme described above can be universally used for any endohedral system.

The remarkable feature of this approach is that for fragment X consisting of more than one atom, calibration curve can be constructed using the 1s orbital energy of any of the atoms of the incarcerated molecule. For example, calibration curves constructed using O 1s orbital energies and N 1s orbital energies for NO@B_{39} complex predict 0.212 e and 0.253 e charge on NO species, respectively (in detail, the procedure for constructing the calibration curves and the charges prediction for denoted NO species and all others considered in this paper is presented in supporting information). An agreement between the results obtained from different calibration curves is a good indicator of reliability of the result. However, it should be emphasized that this charge assessment method does not allow determination of charge on the individual atoms of the encapsulated fragment X, but only provides the charge on the whole fragment. On the other hand, taking into account physical model underlying the method described the following limitations must be noted. First, the proposed model does not take into account orbital interactions. Thus, if orbitals of fragment X are involved in strong orbital interactions, a significant error could be observed. Second, because the compensation charge in our method were treated within the framework of point charge model, a small underestimation of the predicted charge could take a place. The reason for this is that charge associated with particular node of cell is not point charge in fact, but only distributed electron density

located somewhat closer to the fragment X, which in turn, will certainly affect the accuracy of the electrostatic correction.

Conclusions

In conclusion, we have developed a new approach for charge assessment of the encapsulated fragment based on the comparison of the low-lying orbital energies of atoms in central fragment in complex of interest with reference systems. The proposed approach demonstrates excellent performance on endohedral borospherenes $X@B_{39}$ with encapsulated metal atoms, halogens or small radicals. Moreover, the workability of proposed approach has been demonstrated on the typical fullerene based $Sc_3N@I_h$-C_{80} endohedral complex. In view of the physical and computational simplicity, the proposed method can be applied to very large systems. In cases when conventional schemes provide essentially different results, the proposed method could be used as a convenient and robust tool to exclude unreliable data from consideration. We are convinced that the proposed approach will find application in research of all kinds of endohedral complexes and related fields of chemical science.

References

1. Mulliken, R. S. Electronic Population Analysis on LCAO–MO Molecular Wave Functions. I. *J. Chem. Phys.* **23**, 1833–1840, https://doi.org/10.1063/1.1740588 (1955).
2. Löwdin, P. O. On the Non-Orthogonality Problem Connected with the Use of Atomic Wave Functions in the Theory of Molecules and Crystals. *J. Chem. Phys.* **18**, 365–375, https://doi.org/10.1063/1.1747632 (1950).
3. Hirshfeld, F. L. Bonded-atom fragments for describing molecular charge densities. *Theor. Chim. Acta* **44**, 129–138, https://doi.org/10.1007/bf00549096 (1977).
4. Marenich, A. V., Jerome, S. V., Cramer, C. J. & Truhlar, D. G. Charge Model 5: An Extension of Hirshfeld Population Analysis for the Accurate Description of Molecular Interactions in Gaseous and Condensed Phases. *J. Chem. Theory Comput.* **8**, 527–541, https://doi.org/10.1021/ct200866d (2012).
5. Foster, J. P. & Weinhold, F. Natural hybrid orbitals. *J. Am. Chem. Soc.* **102**, 7211–7218, https://doi.org/10.1021/ja00544a007 (1980).
6. Reed, A. E., Weinstock, R. B. & Weinhold, F. Natural population analysis. *J. Chem. Phys.* **83**, 735–746, https://doi.org/10.1063/1.449486 (1985).
7. Bader, R. F. W. *Atoms in Molecules: A Quantum Theory* (Oxford, 1990).
8. Bader, R. F. W. A quantum theory of molecular structure and its applications. *Chem. Rev.* **91**, 893–928, https://doi.org/10.1021/cr00005a013 (1991).
9. Kroto, H. W., Heath, J. R., O'Brien, S. C., Curl, R. F. & Smalley, R. E. C_{60}: Buckminsterfullerene. *Nature* **318**, 162–163, https://doi.org/10.1038/318162a0 (1985).
10. Heath, J. R. *et al.* Lanthanum complexes of spheroidal carbon shells. *J. Am. Chem. Soc.* **107**, 7779–7780, https://doi.org/10.1021/ja00311a102 (1985).
11. Chai, Y. *et al.* Fullerenes with metals inside. *J. Phys. Chem.* **95**, 7564–7568, https://doi.org/10.1021/j100173a002 (1991).
12. Cox, D. M., Trevor, D. J., Reichmann, K. C. & Kaldor, A. C_{60}La: a deflated soccer ball? *J. Am. Chem. Soc.* **108**, 2457–2458, https://doi.org/10.1021/ja00269a060 (1986).
13. Popov, A. A., Yang, S. & Dunsch, L. Endohedral Fullerenes. *Chem. Rev.* **113**, 5989–6113, https://doi.org/10.1021/cr300297r (2013).
14. Castro, E., Hernandez Garcia, A., Zavala, G. & Echegoyen, L. Fullerenes in Biology and Medicine. *J. Mater. Chem. B* **5**, 6523–6536, https://doi.org/10.1039/C7TB00855D (2017).
15. Yang, S., Wei, T. & Jin, F. When metal clusters meet carbon cages: endohedral clusterfullerenes. *Chem. Soc. Rev.* **46**, 5005–5058, https://doi.org/10.1039/C6CS00498A (2017).
16. Lu, X., Akasaka, T. & Nagase, S. Chemistry of endohedral metallofullerenes: the role of metals. *Chem. Commun.* **47**, 5942–5957, https://doi.org/10.1039/C1CC10123D (2011).
17. Yamada, M., Akasaka, T. & Nagase, S. Endohedral Metal Atoms in Pristine and Functionalized Fullerene Cages. *Acc. Chem. Res.* **43**, 92–102, https://doi.org/10.1021/ar900140n (2010).
18. Zhang, J., Stevenson, S. & Dorn, H. C. Trimetallic Nitride Template Endohedral Metallofullerenes: Discovery, Structural Characterization, Reactivity, and Applications. *Acc. Chem. Res.* **46**, 1548–1557, https://doi.org/10.1021/ar300301v (2013).
19. Rudolf, M. *et al.* Endohedral Metallofullerenes—Filled Fullerene Derivatives towards Multifunctional Reaction Center Mimics. *Chem. Eur. J.* **18**, 5136–5148, https://doi.org/10.1002/chem.201102844 (2012).
20. Cerón, M. R., Li, F.-F. & Echegoyen, L. A. Endohedral fullerenes: the importance of electronic, size and shape complementarity between the carbon cages and the corresponding encapsulated clusters. *J. Phys. Org. Chem.* **27**, 258–264, https://doi.org/10.1002/poc.3245 (2014).
21. Garcia-Borràs, M., Osuna, S., Luis, J. M., Swart, M. & Solà, M. The role of aromaticity in determining the molecular structure and reactivity of (endohedral metallo)fullerenes. *Chem. Soc. Rev.* **43**, 5089–5105, https://doi.org/10.1039/C4CS00040D (2014).
22. Popov, A. A. *Endohedral Fullerenes: Electron Transfer and Spin* (Cham, 2017).
23. Shi, Z.-Q., Wu, X., Wang, C.-R., Lu, X. & Shinohara, H. Isolation and Characterization of $Sc_2C_2@C_{68}$: A Metal-Carbide Endofullerene with a Non-IPR Carbon Cage. *Angew. Chem. Int. Ed.* **45**, 2107–2111, https://doi.org/10.1002/anie.200503705 (2006).
24. Stevenson, S. *et al.* Materials science: A stable non-classical metallofullerene family. *Nature* **408**, 427–428, https://doi.org/10.1038/35044199 (2000).
25. Zhai, H.-J. *et al.* Observation of an all-boron fullerene. *Nat. Chem.* **6**, 727–731, https://doi.org/10.1038/nchem.1999 (2014).
26. Bai, H., Chen, Q., Zhai, H.-J. & Li, S.-D. Endohedral and Exohedral Metalloborospherenes: $M@B_{40}$ (M = Ca, Sr) and $M\&B_{40}$ (M = Be, Mg). *Angew. Chem., Int. Ed.* **54**, 941–945, https://doi.org/10.1002/anie.201408738 (2015).
27. Tian, W.-J. *et al.* Saturn-like charge-transfer complexes $Li_4\&B_{36}$, $Li_5\&B_{36}^+$, and $Li_6\&B_{36}^{2+}$: exohedral metalloborospherenes with a perfect cage-like B_{36}^{4-} core. *Phys. Chem. Chem. Phys.* **18**, 9922–9926, https://doi.org/10.1039/C6CP01279E (2016).
28. Chen, Q. *et al.* Endohedral $Ca@B_{38}$: stabilization of a B_{38}^{2-} borospherene dianion by metal encapsulation. *Phys. Chem. Chem. Phys.* **18**, 11610–11615, https://doi.org/10.1039/c5cp06169e (2016).
29. Chen, Q. *et al.* Endohedral $C_3Ca@B_{39}^+$ and $C_2Ca@B_{39}^+$: axially chiral metalloborospherenes based on B_{39}. *Phys. Chem. Chem. Phys.* **17**, 19690–19694, https://doi.org/10.1039/C5CP03178H (2015).
30. Liu, C., Yang, L., Jin, P., Hou, Q. H. & Li, L. L. Computational prediction of endohedral dimetalloborofullerenes $M_2@B_{80}$ (M = Sc, Y). *Chem. Phys. Lett.* **676**, 89–94, https://doi.org/10.1016/j.cplett.2017.03.054 (2017).
31. Li, S. X., Zhang, Z. P., Long, Z. W. & Qin, S. J. Structures, stabilities and spectral properties of borospherene B_{44}^- and metalloborospherenes $MB_{44}^{0/-}$ (M = Li, Na, and K). *Sci. Rep.* **7**, 40081, https://doi.org/10.1038/srep40081 (2017).
32. Xu, Q. H. *et al.* Computational investigation on MB_n (M = Li-Cs, Be-Ba, Sc-La and Ti; n = 28 and 38). *J. Mol. Model.* **22**, 184, https://doi.org/10.1007/s00894-016-3055-4 (2016).
33. Bin, L. *et al.* B_{40} fullerene as a highly sensitive molecular device for NH_3 detection at low bias: a first-principles study. *Nanotechnology* **27**, 075501, https://doi.org/10.1088/0957-4484/27/7/075501 (2016).

34. Stasyuk, A. J. & Solà, M. Does the endohedral borospherene supersalt $FLi_2@B_{39}$ maintain the "super" properties of its subunits? *Phys. Chem. Chem. Phys.* **19**, 21276–21281, https://doi.org/10.1039/C7CP02550E (2017).
35. Kawashima, Y., Ohkubo, K. & Fukuzumi, S. Efficient Charge Separation in $Li^+@C_{60}$ Supramolecular Complexes with Electron Donors. *Chem. - Asian J.* **10**, 44–54, https://doi.org/10.1002/asia.201403075 (2015).
36. Supur, M. *et al.* Graphene oxide- $Li^+@C_{60}$ donor-acceptor composites for photoenergy conversion. *Phys. Chem. Chem. Phys.* **17**, 15732–15738, https://doi.org/10.1039/c5cp01403d (2015).
37. Martinez, J. P., Solà, M. & Voityuk, A. A. The Driving Force of Photoinduced Charge Separation in Metal-Cluster-Encapsulated Triphenylamine-[80]fullerenes. *Chem. - Eur. J.* **22**, 17305–17310, https://doi.org/10.1002/chem.201603504 (2016).
38. Voityuk, A. A. & Solà, M. Photoinduced Charge Separation in the Carbon Nano-Onion $C_{60}@C_{240}$. *J. Phys. Chem. A* **120**, 5798–5804, https://doi.org/10.1021/acs.jpca.6b04127 (2016).
39. Andrae, D., Häußermann, U., Dolg, M., Stoll, H. & Preuß, H. Energy-adjusted ab initio pseudopotentials for the second and third row transition elements. *Theor. Chim. Acta* **77**, 123–141, https://doi.org/10.1007/BF01114537 (1990).
40. Adamo, C. & Barone, V. Toward reliable density functional methods without adjustable parameters: The PBE0 model. *J. Chem. Phys.* **110**, 6158–6170, https://doi.org/10.1063/1.478522 (1999).
41. Weigend, F. & Ahlrichs, R. Balanced basis sets of split valence, triple zeta valence and quadruple zeta valence quality for H to Rn: Design and assessment of accuracy. *Phys. Chem. Chem. Phys.* **7**, 3297–3305, https://doi.org/10.1039/B508541A (2005).
42. Weigend, F. Accurate Coulomb-fitting basis sets for H to Rn. *Phys. Chem. Chem. Phys.* **8**, 1057–1065, https://doi.org/10.1039/B515623H (2006).
43. Gaussian 09 Rev. E.01. (full citation in ESI).
44. Berzinsh, U. *et al.* Isotope shift in the electron affinity of chlorine. *Phys. Rev. A* **51**, 231–238, https://doi.org/10.1103/PhysRevA.51.231 (1995).
45. Chen, Q. *et al.* Experimental and Theoretical Evidence of an Axially Chiral Borospherene. *ACS Nano* **9**, 754–760, https://doi.org/10.1021/nn506262c (2015).
46. Slegbahn, K. *et al. ESCA Atomic, Molecular and Solid State Structure Studied by Means of Electron Spectroscopy* (Uppsala, 1967).
47. Slegbahn, K. *et al. ESCA Applied to Free Molecules* (Amsterdam/London, 1969).
48. Bagus, P. S., Ilton, E. S. & Nelin, C. J. The interpretation of XPS spectra: Insights into materials properties. *Surf. Sci. Rep.* **68**, 273–304, https://doi.org/10.1016/j.surfrep.2013.03.001 (2013).
49. Lopes, P. E. M., Roux, B. & MacKerell, A. D. Molecular modeling and dynamics studies with explicit inclusion of electronic polarizability: theory and applications. *Theor. Chem. Acc.* **124**, 11–28, https://doi.org/10.1007/s00214-009-0617-x (2009).
50. Tsunekawa, S., Sahara, R., Kawazoe, Y. & Kasuya, A. Origin of the blue shift in ultraviolet absorption spectra of nanocrystalline CeO_{2-x} particles. *Mater. Trans., JIM* **41**, 1104–1107 (2000).
51. Stevenson, S. *et al.* Small-bandgap endohedral metallofullerenes in high yield and purity. *Nature* **401**, 55–57, https://doi.org/10.1038/43415 (1999).
52. Iezzi, E. B. *et al.* A Symmetric Derivative of the Trimetallic Nitride Endohedral Metallofullerene, $Sc_3N@C_{80}$. *J. Am. Chem. Soc.* **124**, 524–525, https://doi.org/10.1021/ja0171005 (2002).
53. Cardona, C. M., Elliott, B. & Echegoyen, L. Unexpected Chemical and Electrochemical Properties of $M_3N@C_{80}$ (M = Sc, Y, Er). *J. Am. Chem. Soc.* **128**, 6480–6485, https://doi.org/10.1021/ja061035n (2006).
54. Garcia-Borràs, M., Osuna, S., Luis, J. M., Swart, M. & Solà, M. A Complete Guide on the Influence of Metal Clusters in the Diels–Alder Regioselectivity of I_h-C_{80} Endohedral Metallofullerenes. *Chem. - Eur. J.* **19**, 14931–14940, https://doi.org/10.1002/chem.201302202 (2013).
55. Aroua, S., Garcia-Borràs, M., Osuna, S. & Yamakoshi, Y. Essential Factors for Control of the Equilibrium in the Reversible Rearrangement of $M_3N@I_h$-C_{80} Fulleropyrrolidines: Exohedral Functional Groups versus Endohedral Metal Clusters. *Chem. - Eur. J.* **20**, 14032–14039, https://doi.org/10.1002/chem.201403743 (2014).

Acknowledgements

We are grateful for financial support from the Spanish MINECO (CTQ2017-85341-P and CTQ2015-69363-P projects), the Catalan DIUE (2014SGR931, XRQTC, and ICREA Academia 2014 Award to M.S.), and the FEDER fund (UNGI10-4E-801). A. J. S. gratefully acknowledges The Interdisciplinary Centre for Mathematical and Molecular Modelling of the University of Warsaw (ICM) for computational facilities (grant no. G33-17).

Author Contributions

A.J.S., M.S. and A.A.V. conceived and designed research, analyzed data, interpreted results and wrote the paper. A.J.S. performed the calculations.

Additional Information

Supplementary information accompanies this paper at https://doi.org/10.1038/s41598-018-21240-0.

Competing Interests: The authors declare no competing interests.

Publisher's note: Springer Nature remains neutral with regard to jurisdictional claims in published maps and institutional affiliations.